

# Ice Thickness Derived From High-Resolution Radar Imagery

A new analysis makes it possible to produce basin-scale estimates of sea ice age and thickness from observations of ice motion in radar images of the Arctic Ocean. Anticipated from sequential synthetic aperture radar (SAR) imagery over a series of winters are Arctic-wide fields of ice motion and estimates of ice age and thickness. This analysis technique is implemented in the RADARSAT Geophysical Processor System (RGPS), a data processing system dedicated to analyzing large volumes of SAR imagery of sea ice [Kwok, 1998].

Currently, we have only crude estimates on how much ice there is, how it varies in space and time, where ice is produced and where it melts, and how rapidly it is transported from place to place. SAR provides an amazingly detailed look at sea ice, but the level of detail is so great that it is not at first apparent how to utilize the data for improving sea ice data sets and models.

RGPS is offered as a solution to this conundrum. It takes over 400 wide-swath radar images every 24-day cycle and produces gridded fields of ice motion, deformation, and thickness. The sea ice thickness distribution is an essential descriptor of the Arctic Ocean sea ice mass and heat balance and is a record of the interplay between dynamics (lead formation, ridging, and advection) and thermodynamics (ice growth and melt).

These geophysical products can be put to a variety of uses, such as analyzing new ice climatologies and testing ice models or new ideas about sea ice rheology. They also can be assimilated into sea ice models.

Our present knowledge of Arctic ice thickness distribution is derived largely from analyses of sonar data from submarine cruises. Moored upward-looking sonars have also been used to sample the thickness distribution at fixed locations. However, these observations do not provide a complete spatial picture or continual updates of the distribution.

The new analysis technique allows us to monitor the spatial and temporal variability of the thin ice distribution (< 2 m) in the Arctic Ocean using high-resolution SAR imagery. This new method estimates ice age and thickness from repeated observations of Lagrangian elements or cells of sea ice in sequential SAR imagery.

Figure 1 shows the time series of observations of one cell within a matrix of such cells, graphs of the history of cell area, and the thin ice coverage within that cell at the end of a 41-day period. Line segments connecting the four

vertices of a cell define its boundaries. The drift and deformation of a cell over time are obtained by tracking the displacement of its vertices in the SAR imagery. The motion tracking procedure is described by Kwok et al. [1995].

The age histogram of the ice in a cell is computed from the temporal record of area changes. An age histogram of sea ice specifies the fractional area covered by ice of different chronological ages. Every time a new observation is available, we interpret a positive area change as the creation of an area of open water. New ice is assumed to grow over this area immediately after opening. The uncertainty of the ice age occupying this area is dependent on the time interval between observations. This age range is recorded as a new age category in the histogram. At the same time a new category is introduced, existing age categories are "aged" by the same time interval. In Figure 1, this procedure created five ice age categories from the sequence of positive area changes since Day 335.

## Youngest Ice in Cell

A negative change is assumed to have ridged the youngest ice in the cell, reducing its area. The assumption is that once ridging starts, deformation tends to be localized in the recently formed thinner and weaker ice in leads. This area of ridged ice is tracked as a separate category in the age histogram. Ice age is converted to ice thickness using an empirical ice growth formula. Growth rate is approximated as a function of the number of freezing-degree days (FDD) associated with each age category using Lebedev's parameterization (discussed by Maykut [1986]) with  $H = 1.33 F^{0.58}$ , where  $H$  is thickness and  $F$  is the accumulated FDD of that category. Volume is conserved when ice is ridged. All ridged ice is assumed to be five times its original thickness and to occupy a quarter of the area [Parmerter and Coon, 1972].

The scheme is started at fall freeze-up by covering the entire Arctic Ocean with initial 10 x 10 km square elements, except near the ice margins where 25 x 25 km are used. Complete coverage of the Arctic takes approximately 70,000 cells. At start-up, the ice age/thickness histograms within the cells are unknown. In the process described, the ice volume created over a season is recorded in the thin ice thickness distribution and the ridge volumes. Since

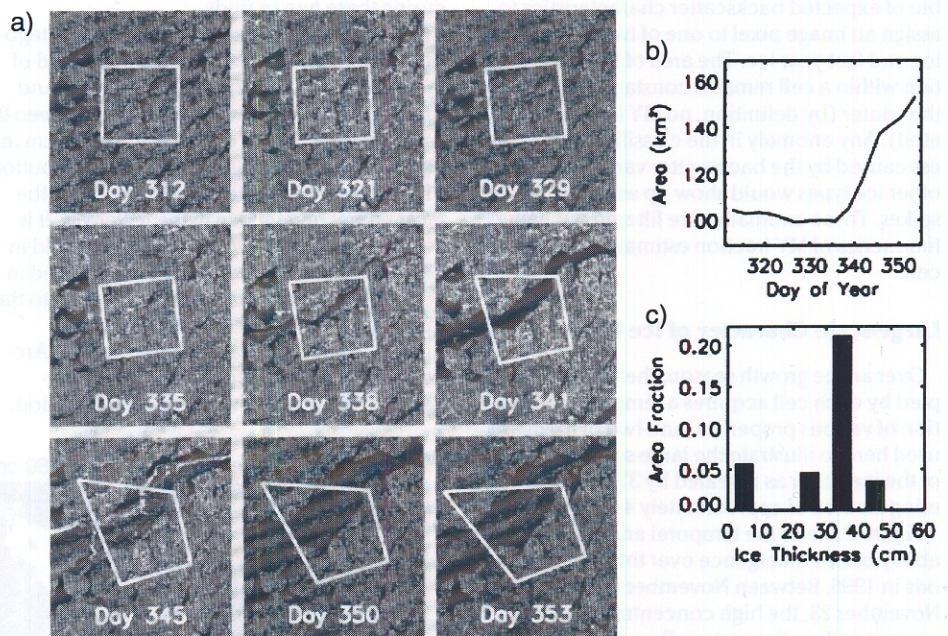


Fig. 1. Time series observations of one Lagrangian element (initially enclosed by a 10 x 10 km square) in RADARSAT imagery. a) The deformation of a cell over a period of 41 days. The area of the cell stays fairly constant until Day 338 when a lead opens. The same lead continued to open between Days 341 and 345, contributing new ice area and ice categories to the cell. At the end of the 41-day period, the area of the thin ice occupies more than 50% of the total cell area. b) The history of the area of the cell. c) The thin ice categories occupying the new areas created since Day 312. The largest thin ice category was created between Days 341 and 345 (RADARSAT imagery, Copyright CSA, 1999).

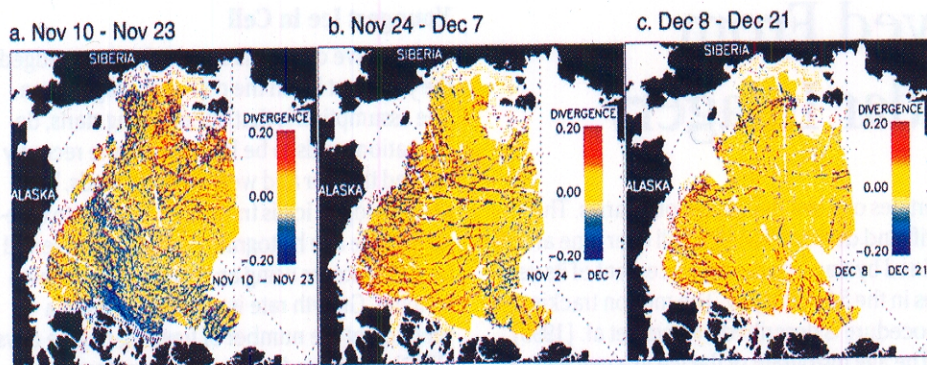


Fig. 2. Cell divergence over three 14-day periods in the winter of 1996. a) November 10 through November 23. b) November 24 through December 7. c) December 8 through December 21. Red indicates divergence while blue indicates convergence.

we do not melt ice in our scheme, the procedures above work only during the winter ice growth season. The results provide fine age/thickness resolution of only the young/thin end of the age/thickness distributions, but this is the crucial range that produces the most ice growth, the most turbulent heat flux to the atmosphere, and the most salt flux to the ocean.

The backscatter intensity of each SAR sample is used to provide an independent estimate of the multiyear (MY) fraction within each cell. The MY algorithm [Kwok *et al.*, 1995] uses a maximum likelihood classifier and a lookup table of expected backscatter characteristics to assign an image pixel to one of two classes: MY ice and first year ice. The area of MY ice fraction within a cell remains constant throughout the winter (by definition, no MY ice is created). Any anomaly in the classification process caused by the backscatter variability of other ice types would show up as transients or spikes. These anomalies are filtered out in the time series of MY fraction estimates in each cell.

### Large-scale Character of Ice Cover

Over an ice growth season, the area occupied by each cell acquires a temporal description of various properties, and two of them are used here to illustrate the large-scale character of the ice cover as revealed by 37,000 cells covering an area of approximately  $4 \times 10^6 \text{ km}^2$ .

Figure 2 shows the temporal and spatial variability of cell divergence over three 14-day periods in 1996. Between November 10 and November 23, the high concentration of convergent cells in the eastern Beaufort Sea above  $75^\circ\text{N}$  adjacent to the Canadian Archipelago and the Greenland coast indicate extensive pressure ridging of the ice cover. In contrast, the eastern Arctic toward Siberia has a more divergent character. Because of the convergence, the sampled ice cover lost approximately 3.5% of its area over this period.

The next period, November 24 through December 7, shows very distinctive diamond-shaped lead patterns over the ice cover. Except for the regions near the ice margin, all the deformation is localized along leads while the rest of the ice cover remains unaffected. The length of some of the leads is quite remarkable, and several leads can be seen to span a large fraction of the Arctic Ocean. The entire ice cover, except for the openings along the margin of the Beaufort Sea, stayed fairly quiescent with minimal lead activity during the last period, December 8-21. The area of the sampled ice cover increased by 2% and 1% during these two periods.

Figure 3 shows the coverage of three categories of thin ice on December 21, at the end of the third period. Approximately 3%, 5%, and 1% of the area is covered by sea ice between 0 and 30 cm, 30 and 60 cm, and 60 and 90 cm in thickness, respectively. The spatial distribution of the thinnest ice category is a record of the most recent divergence in the ice cover. It is highly correlated with the divergence field in Figure 2c. Only lead ice that has not ridged in convergent events can survive to grow into the thicker ice. There is a distinct absence of thicker (60-90 cm) sea ice in the western Arctic, probably due to the extensive convergence of the ice cover during the first period.

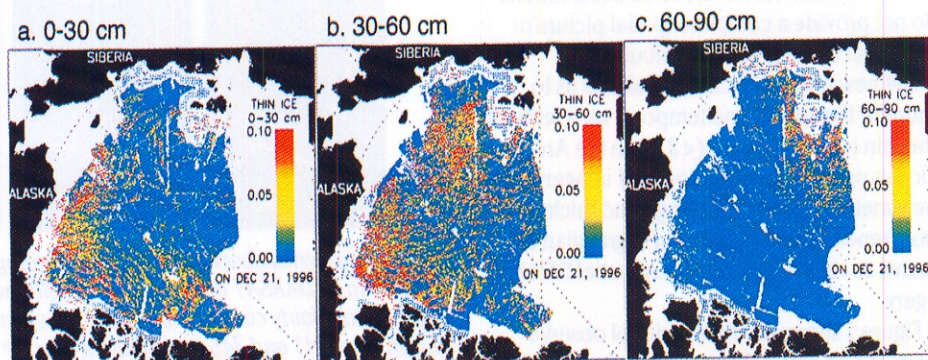


Fig. 3. Thin ice coverage on December 21, 1996. a) 0-30 cm; b) 30-60 cm; c) 60-90 cm. The colors indicate the fraction of each cell covered by thin ice in that thickness range. For example, in Panel a, red indicates that 10% of the cell is covered by ice 0-30 cm thick.

On December 21, 1996, approximately 3.5% of the area was covered by ridged ice formed during the 41 days.

### Launched in 1995

Canada's RADARSAT satellite was launched in November 1995 into a 24-day repeat cycle, an orbit configuration that provides near-repeat coverage of the high latitudes at 3- and 7-day intervals. The C-band (5.3 GHz) radar has an imaging mode that illuminates a wide swath (460 km) and is well suited for large-scale mapping of the Earth's surface. To support the data needs of RGPS, we have been using this mode, termed ScanSAR, to acquire repeat coverage of the Arctic Ocean since November 1996.

Over a 24-day repeat cycle of the satellite, we have close to eight observations of the western Arctic Ocean within the Alaska SAR Facility (ASF) reception mask in Fairbanks. The repeat coverage of the Eurasian Basin is less frequent (6 days) due to the additional cost of RADARSAT data downlinked at the Tromsø Satellite Station in Norway. We expect to continue this acquisition process over the life of the RADARSAT mission. The input SAR imagery is processed to a spatial resolution approximately  $100 \times 100 \text{ m}$ , and is calibrated and archived at ASF.

Overall, RGPS produces Lagrangian ice drift information; ice age and thickness histograms; backscatter and ice deformation data; and the dates of melt onset and freeze-up. These data contain ice motion of the vertices of the cells as well as the ice age/thickness histograms of each cell. The distribution of backscatter within each cell is stored as histograms. Ice deformation is the divergence, shear, and vorticity of a cell derived from velocity gradients computed from ice motion at the cell vertices. The dates of spring melt and fall freeze are detected by changes in the backscatter record of each cell [Winebrenner *et al.*, 1998].

The RGPS Science Working Group addresses issues on product and algorithm development and product validation. Validation of the ice

thickness products is currently being undertaken by a number of investigators using data sets from upward-looking sonars (moored and submarine), other remote sensing data sets (advanced very high resolution radiometer and passive microwave), and numerical model simulations. The activities of the working group can be found on the Web (<http://www-radar.jpl.nasa.gov/rgps>).

More than 2 years of almost continuous observations of the Arctic Ocean have been acquired with RADARSAT so far. Processing of imagery commenced in January 1999. The current throughput is approximately one cycle of data (over 400 frames) every 30 days. The intention is to eventually process all the RADARSAT data of the Arctic Ocean in the ASF archive.

At this time, we have processed more than five cycles (120 days) of RADARSAT data acquired between November 1995 and February 1996. With the addition of a new system later

this year, our effective throughput will increase to one cycle every 15 days. We expect to complete processing the 1996-1997 winter data in December 1999. Processing the 1997-1998 winter data began in June 1999. Currently, the data products, documentation, and software for reading the products are available on the Web site mentioned above. The site also contains animation sequences of deformation fields. Later this year as more RGPS products are generated, they will become available through the EOS Data Gateway as well.

#### Authors

*Ron Kwok, Glenn F. Cunningham, Nettie LaBelle-Hamer, Benjamin Holt, and Drew Rothrock*

For more information, contact Ron Kwok, Jet Propulsion Laboratory, MS 300-235, 4800 Oak Grove Dr., Pasadena CA 91109 USA; E-mail: [ron@rgps1.jpl.nasa.gov](mailto:ron@rgps1.jpl.nasa.gov)

#### References

- Kwok, R., D. A. Rothrock, H. L. Stern, and G. F. Cunningham, Determination of Ice Age using Lagrangian observations of ice motion, *IEEE Trans. Geosci. Remote Sens.*, *33*, 392-400, 1995.
- Kwok, R., The RADARSAT Geophysical Processor System, in *Analysis of SAR data of the Polar Oceans: Recent Advances*, edited by C. Tsatsoulis and R. Kwok, pp. 235-258, Springer-Verlag, New York, 1998.
- Maykut, G. A., The Surface Heat and Mass Balance, in *Geophysics of Sea Ice, NATO ASI Ser., Ser. B Phys., vol. 146*, edited by N. Untersteiner, pp. 395-463, Plenum, New York, 1986.
- Parmeter, R. R., and M. Coon, Model of pressure ridge formation in sea ice, *J. Geophys. Res.*, *77*, 6565-6575, 1972.
- Winebrenner, D. P., D. G. Long, and B. Holt, Mapping the progression of melt onset and freeze-up on Arctic sea ice using SAR and scatterometry, in *Analysis of SAR data of the Polar Oceans: Recent Advances*, edited by C. Tsatsoulis and R. Kwok, pp. 129-144, Springer-Verlag, New York, 1998.